Shear-Driven Failure of Liquid-Infused Surfaces

Jason S. Wexler, Ian Jacobi, and Howard A. Stone

Phys. Rev. Lett. **114**, 168301 — Published 22 April 2015

DOI: 10.1103/PhysRevLett.114.168301

Shear-driven failure of liquid-infused surfaces

Jason S. Wexler,[1] Ian Jacobi,[1,2] and Howard A. Stone[1,*]

[1] *Department of Mechanical and Aerospace Engineering, Princeton University, Princeton, New Jersey 08544, USA*

[2] *Faculty of Aerospace Engineering, Technion – Israel Institute of Technology, Haifa 32000 Israel*

Rough or patterned surfaces infused with a lubricating liquid display many of the same useful properties as conventional gas-cushioned superhydrophobic surfaces. However, liquid-infused surfaces exhibit a new failure mode: the infused liquid film may drain due to an external shear flow, causing the surface to lose its advantageous properties. We examine shear-driven drainage of liquid-infused surfaces with the goal of understanding and thereby mitigating this failure mode. On patterned surfaces exposed to a known shear stress, we find that a finite length of the surface remains wetted indefinitely, despite the fact that no physical barriers prevent drainage. We develop an analytical model to explain our experimental results, and find that the steady-state retention results from the ability of patterned surfaces to wick wetting liquids, and is thus analogous to capillary rise. We establish the geometric surface parameters governing fluid retention and show how these parameters can describe even random substrate patterns.

PACS numbers: 68.08.Bc, 68.35.Ct, 47.15.gm, 47.60.Dx

Liquid-infused surfaces demonstrate a remarkable array of useful properties, from omniphobicity [1–3] and bio-fouling resistance [4], to enhanced heat transfer [5, 6] and drag reduction [7–9]. Unlike traditional superhydrophobic materials, liquid-infused surfaces are robust against pressure-induced failure, making them particularly attractive for submerged applications [10–16]. However, when these surfaces are immersed in dynamic fluid environments, external flow can shear away the infused liquid layer that is responsible for their unique properties.

Robust implementation of liquid-infused surfaces thus requires a thorough understanding of the dynamics of a liquid lubricant trapped within a patterned substrate that is exposed to shear. This fundamental shear-driven drainage problem also applies to a wide variety of structurally similar situations, including cleaning oily surface contaminants from textiles [17], extraction of residual oil from permeable rocks [18], liquid-vapor interactions in micro-patterned heat pipes [19, 20], and the shear flow over hydrophobic mucus trapped on rough biological tissue [21, 22]. Existing theories that govern liquid films trapped in rough or patterned surfaces are able to describe the process of imbibition [23–26], the flow of a superficial fluid film above the height of the underlying surface pattern [27, 28], and the static configurations of wetting drops [29]. In addition, the steady-state shape of a shear- or gravity-driven film that coats individual surface features has been explored [30–33]. Despite these advances, current theories are unable to predict whether a patterned surface will retain an infused liquid when subject to an external flow.

We report a series of experiments to study the behavior of liquid-infused patterned surfaces exposed to the flow of an immiscible liquid. A microfluidic flow cell was constructed from transparent epoxy [34] with a patterned surface imprinted on a section of its floor (Fig. 1(a)-(c)). The surface pattern in this experiment consists of 50 streamwise grooves with width $w = 8.8 - 9.2$ µm and height $h = 10.0$ µm (Fig. 1(d)) that end upstream in a 1 mm by 1 mm well of equal depth to create the open end shown schematically in Fig. 2(c). The pattern is initially filled with silicone oil mixed with fluorescent dye (viscosity $\mu_o = 42.7$ or 201 mPa·s), and connects to a downstream reservoir of oil at the terminus of the flow cell. The external aqueous fluid (a 1:1 wt. mixture of glycerol and water, viscosity $\mu_{aq} = 5.4$ mPa·s) enters the upstream inlet of the device, and exits through a slot-shaped outlet that is upstream of the terminus. This configuration ensures that the draining oil does not block the flow of the external phase, and that the external flow is not constricted as it exits the device. The flow cell (height $H = 180$ µm and width $W = 7$ mm) is thin but still much deeper than the pattern, so that the flow profile is approximately parabolic through its depth and uniform through its width. Thus a flow rate Q imposes a shear stress $\tau_{yx} = 6\mu_{aq}Q/WH^2$ on the pattern.

Using micro-fabricated grooves to study lubricant drainage ensures a controlled and reproducible surface topography that is invariant in the streamwise direction, thereby providing a system amenable to a fluid dynamical description. The lessons learned from studying this geometry can be applied to predicting the drainage behavior of surfaces with more complicated topographies, as we demonstrate below. Indeed, there is a strong precedent in the study of capillary flows for such a 'reduced-order' approach to treating complicated geometries [23, 28]. The particular geometry of streamwise grooves also represents what appears to be the 'worst-case' surface configuration for oil retention. This worst-case scenario is instructive for evaluating many real-world liquid-infused surfaces, since rough surfaces inevitably have some degree of streamwise connectivity – either by accident or

by design – that allows fluid in upstream portions of the pattern to drain downstream.

The behavior of the oil phase was observed using fluorescence macro photography. A time series of photographs from a typical experiment is shown in Fig. 1(c), demonstrating the characteristic drainage behavior (see Movie 1): under the influence of shear from the aqueous phase, the oil in the upstream portion of the pattern dewets first, with a dewetting front that propagates downstream. The front initially propagates rapidly, before slowing and eventually stopping at a steady-state streamwise position; the length of fluid retained in the pattern between this final front location and the slot-shaped outlet is defined as the steady-state length, L_∞ (Fig. 1(c)).

Since the streamwise grooves terminate in a fluid reservoir, there is no physical barrier to drainage of the oil, and thus the existence of steady-state oil retention may seem non-intuitive. To clarify the mechanism that leads to

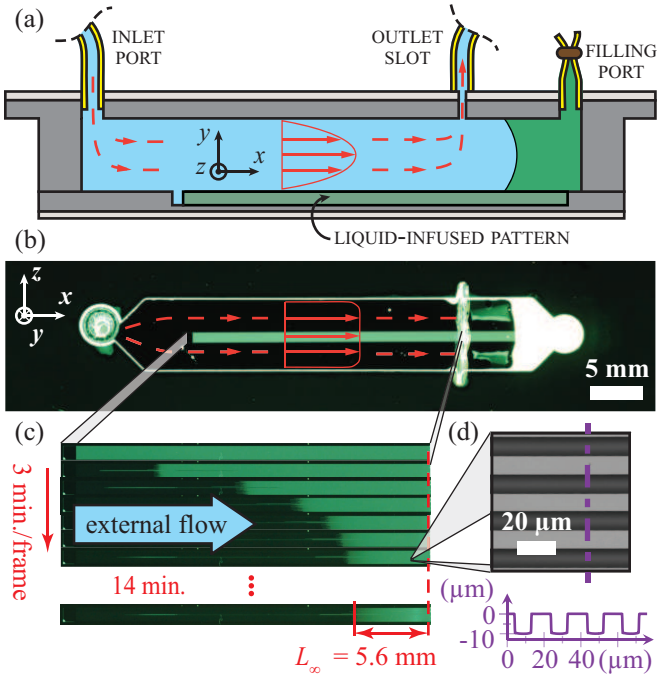

FIG. 1. (a) Cross-section of the microfluidic flow cell, showing the configuration at the beginning of an experiment. Distances in the y-direction are exaggerated. The aqueous solution (blue) flows in the left inlet and out the first (slot-shaped) outlet. The grooves are filled with oil (green), and connect to the reservoir of oil at the flow cell terminus. (b) This planform view shows the entire device before drainage commences. Low viscosity oil fills the 50 longitudinal grooves at the center of the device and fluoresces green. (c) Snapshots of a sample shear-driven drainage experiment subject to an aqueous flow of $Q = 2$ mL/min ($\tau_{yx} = 5.2$ Pa). (d) Micrograph of the silicon wafer micro-pattern that is used to mold the grooves, including the surface profile (purple). Grooves appear dark gray and walls appear light gray.

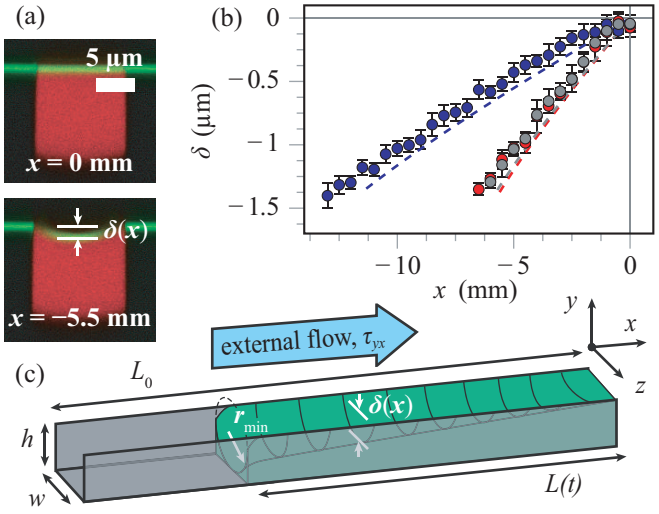

FIG. 2. (a) Representative groove cross-sections from the steady-state configuration of an experiment conducted at $Q = 2$ mL/min with low viscosity oil, taken at the outlet slot ($x = 0$ mm) and the far upstream end of the wetted groove ($x = -5.5$ mm). (b) The steady-state deflection at the center of the groove, $\delta(x)$, with theoretical predictions (Supplemental Material) plotted as dashed lines. Gray is low viscosity oil at $Q = 2$ mL/min, red is high viscosity oil at the same flow rate, and blue is low viscosity oil at $Q = 1$ mL/min. (c) Schematic of one groove, showing geometric parameters and the shape of the interface deduced from (b).

oil retention, we perform identical experiments using a confocal microscope, and observe the steady-state configuration of the oil at the scale of the pattern itself. Cross-sectional (yz-plane) images of the steady-state oil distribution are taken at regular intervals in the streamwise (x) direction along the length of the filled portion of the groove. Two representative images are shown in Fig. 2(a). The fluorescent oil (represented as red) is index-matched with the solid so that the interface between the oil/solid and aqueous phase is visible in reflection (represented as green).

The oil-aqueous interface is deflected inward towards the substrate and appears to have a constant curvature, κ, in the cross-sectional (yz) plane. Because the length of the filled portion of the groove is much longer than the width or height of the groove, this cross-sectional interfacial curvature dominates over curvature in the streamwise/wall-normal (xy) plane. The pressure drop across a curved liquid-liquid interface is equal to κ multiplied by the surface tension of the interface, γ. Since the interface is deflected inwards, the pressure is lower in the oil than in the aqueous phase. Thus, the pressure within the oil decreases in the direction opposite the flow of the external phase. This adverse pressure gradient drives recirculation of the oil trapped in the groove, countering the external shear stress, and provides the physical mechanism for a steady-state wetting configuration un-

der shear.

We note that this explanation of the oil retention mechanism rests on a number of assumptions about the system: the Reynolds number in the oil $\rho_o \tau_{yx} h^2/\mu_o^2 \ll 1$, indicating negligible inertial effects, and the Bond number $w^2 g(\rho_{aq} - \rho_o)/\gamma \ll 1$, indicating that gravity is negligible. These assumptions apply to most applications of liquid-infused surfaces. Furthermore, we ignore long-range forces (such as van der Waals); though this assumption is valid for the micro-scale patterns of the current experiment, long-range forces may be relevant for certain chemistries on surfaces with nano-scale geometries. Finally, we assume that $\mu_o \gg \mu_{aq}$, so that the shear stress imposed by the aqueous flow is effectively unchanged by the oil.

The adverse pressure gradient driving oil in the upstream direction depends on the gradient in curvature of the interface over the length of the groove. At the downstream end, where the aqueous fluid exits the flow cell, the interface is flat, indicating zero pressure drop across the interface. At the upstream end, the minimum radius of curvature, r_{min}, is determined by the groove width, w, and the receding contact angle, θ, or, for wider grooves, the aspect ratio of the groove, w/h. The interfacial deflection at the groove center, δ, varies as $\delta \sim x$ between these two limits, as shown in Fig. 2(b). Since $\delta \sim \kappa$ for small deflections, $d\kappa/dx$ is approximately constant, indicating that the pressure gradient within the oil is constant.

We now construct a quantitative model to predict the dynamics of drainage from the grooved pattern based on the flow reversal mechanism we inferred from interfacial measurements. Our goal is to predict how the wetted length of the groove, $L(t)$, evolves under the action of an applied shear stress, τ_{yx}. The most direct approach to determining $L(t)$ is to develop a volume-balance conservation equation for the flux of oil out of the groove. Details of the derivation are provided in the Supplemental Material [35], but we outline the model now.

The time derivative of the volume of oil in a groove of filled length $L(t)$ is given by $c_d wh\, dL/dt$, where c_d is a constant that depends on the aspect ratio of the groove, w/h, and represents the average fraction of the groove's cross-section, wh, that is oil-filled. This time derivative must equal the sum of the downstream flux of oil driven by shear and the upstream flux of oil driven by the pressure gradient. The oil flux induced by a shear stress τ_{yx} is given by $-c_s \tau_{yx} wh^2/\mu_o$, where the sign indicates that the flux acts to decrease the volume of oil in the groove. The constant c_s depends on the aspect ratio w/h, and accounts for the hydrodynamic resistance imposed by the walls and floor of the groove. The flux of oil driven upstream by the pressure gradient can be related to the change in interfacial curvature over the wetted length of the groove, as described above. The total pressure drop is proportional to $1/r_{min}$; the pressure gradient is distributed along the oil-filled length and is therefore proportional to $1/L$. Thus, the pressure-driven recirculation flux is given by $c_p wh^3\gamma/(\mu_o r_{min} L)$, where c_p is another hydrodynamic resistance constant dependent on w/h. Summing these three terms to enforce volume conservation yields

$$c_d wh \frac{dL}{dt} = -\frac{c_s \tau_{yx} wh^2}{\mu_o} + \frac{c_p wh^3 \gamma}{\mu_o r_{min}} \frac{1}{L}. \quad (1)$$

The steady-state length of oil, L_∞, is found by setting the left-hand side of Eq. (1) equal to zero, yielding

$$L_\infty = \left(\frac{c_p h}{c_s r_{min}}\right) \frac{\gamma}{\tau_{yx}}, \quad (2)$$

where the pre-factor contains all effects of the groove geometry. Using L_∞ as a length-scale for non-dimensionalizing Eq. (1), a corresponding time-scale is $t_c = c_d c_p \mu_o \gamma/(c_s^2 r_{min} \tau_{yx}^2)$, thus yielding a non-dimensional ordinary differential equation with no free parameters; this equation appears in the same form as the Lucas-Washburn equation that describes the dynamics of capillary rise [36, 37]. Thus, L_∞ is a shear-driven equivalent to the classical capillary rise height, and results from the ability of patterned surfaces to wick wetting fluids.

The proposed model for groove drainage was validated against macroscale measurements of how the wetted length of the grooves changes as a function of time. Fig. 3(a)-(b) show the measured drainage behavior at two different shear rates, and how the non-dimensional scales collapse both drainage trends towards the universal theoretical prediction. An important consequence of the analysis is that the steady-state length, L_∞, does not depend on the viscosity of the fluid in the groove, μ_o (see Eq. (2)). Thus, μ_o can be used as a design parameter in the construction of liquid-infused materials without influencing the oil retention properties. The viscosity independence was validated by repeating the above experiments with two different oils whose viscosities differ by an order of magnitude. Despite the different drainage rates between the two oils, the steady-state wetted lengths were roughly the same, as shown in Fig. 3(c)-(d).

Another significant design consequence is that the steady-state length is independent of the groove size. Though the groove aspect ratio enters the formula for L_∞, through c_p, c_s, and h/r_{min}, the *magnitude* of the groove size is not important. Grooves with the same aspect ratio should have identical steady-state lengths, regardless of whether the depth is 1 µm or 1 mm. However, when w or h falls into the nano-scale range, long-range forces may modify the retention behavior; conversely, if these dimensions or τ_{yx} become too large, the Reynolds number or Bond number may no longer be low enough for our analysis to remain valid.

Within the parameter range of our analysis, L_∞ depends on only the surface tension, contact angle (through

$r_{\min}$), and groove aspect ratio, so that options for designing a surface to retain lubricant are limited. In most cases, the surface tension and the contact angle cannot be considered adjustable parameters because of the need to prevent the oil from "cloaking" sessile drops [2, 3, 38, 39]. Thus, the aspect ratio of the grooves, w/h, is the primary means of tuning oil retention, and the steady-state length in Eq. (2) depends strongly on this parameter.

To explore the dependence of drainage behavior on aspect ratio, surfaces with grooves of different width and different depth were fabricated and tested at three flow rates (see Supplemental Material). The steady-state length, L_∞, is plotted in Fig. 4(a) along with the theoretical prediction, where L_∞ has been normalized by γ/τ_{yx} in order to isolate effects of the aspect ratio. These results demonstrate that narrower and deeper grooves result in longer L_∞. Fig. 4(b) shows how c_p and c_s vary as a function of w/h. Note that $2/3 < c_p/c_s < 1$, so that groove geometry affects L_∞ in Fig. 4(a) primarily through $h/r_{\min}$.

We noted earlier that longitudinal grooves provide a 'reduced-order' perspective on a variety of more complicated patterned surfaces, and thus we expect surfaces with a random pattern to follow a similar drainage behavior. To demonstrate the general nature of our findings, we repeated the drainage experiments on a surface with a micro-fabricated geometry consisting of randomly placed 10-µm cubes. The film drains from the random posts following a similar behavior: as with the grooves, a finite length of the pattern remains fully wetted (see Fig. 5 and Movie 2). The retention of fluid under shear is therefore not unique to well-controlled surface geometries, and may be expected on surfaces with industrially fabricated patterns that are inherently more random.

Our findings suggest a methodology for designing liquid-infused materials capable of retaining their lubricant up to a design-limited shear stress. We have shown that the value of this limiting shear can be tuned by manipulating the aspect ratio of the surface pattern. Extrapolating further, the theory suggests a method by which

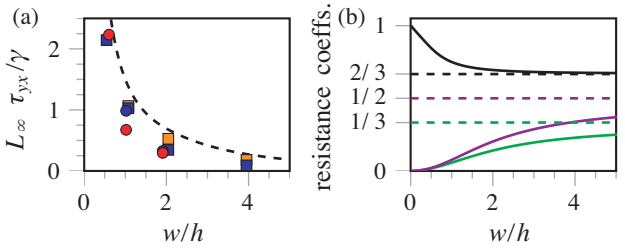

FIG. 4. (a) Steady-state length, L_∞, normalized by γ/τ_{yx}, for varying groove aspect ratio, with low viscosity oil; $Q = 2$ mL/min (red), $Q = 1$ mL/min (blue), and $Q = 0.5$ mL/min (orange). Squares are for grooves with $h \approx 10$ µm, and circles are for grooves with $h \approx 20$ µm. The theoretical prediction from Eq. (2), $L_\infty\,\tau_{yx}/\gamma = 2c_p h/c_s r_{\min}$ is given by the dashed line. (b) Groove resistance coefficients c_p (green), c_s (purple), and the ratio c_p/c_s (black) as a function of aspect ratio w/h. Each curve asymptotes to the dashed line of the same color.

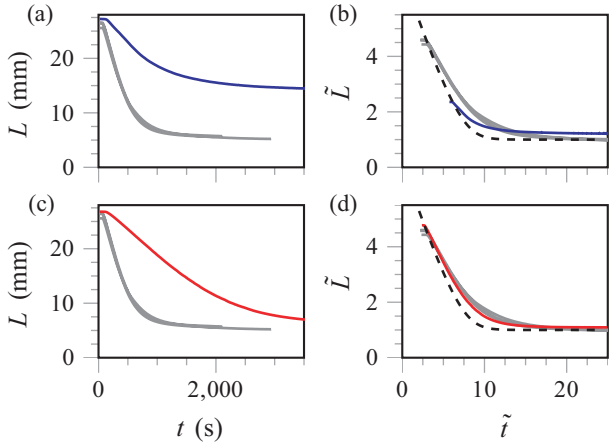

FIG. 3. Drainage curves for grooves, plotted as length versus time, with dimensional results in (a,c) and non-dimensional results in (b,d). Gray is low viscosity oil at $Q = 2$ mL/min, red is high viscosity oil at the same flow rate, and blue is low viscosity oil at $Q = 1$ mL/min. The theoretical prediction from the Supplemental Material is plotted in dashed black. Top row (a,b) shows the effect of varying flow rate and bottom row (c,d) shows the effect of varying the oil viscosity. Each line represents the average wetted length of all of the defect-free grooves from one experiment. Most experiments contain surface defects that cause multiple grooves to drain with a different behavior ($\approx 5 - 10$ of the 50 grooves in each experiment); these grooves are excluded from the averaging. The plot includes multiple experiments conducted with low viscosity oil at the higher flow rate in order to indicate the degree of natural variability in the data.

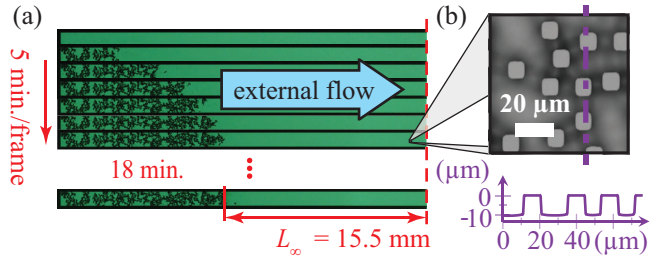

FIG. 5. (a) Snapshots of a shear-driven drainage experiment on a substrate consisting of randomly placed posts. A script was written in MATLAB to define the uniformly random locations of the cubes on a 1-µm grid subject to two conditions: 1) that the area density of the posts is 25%, and 2) that the minimum space between posts is 3 µm (to aid with photolithography). The pattern is initially filled completely with low viscosity oil (green). The oil drains due to an external aqueous flow of $Q = 0.5$ mL/min. (b) Micrograph of the silicon wafer micro-pattern that is used to mold the posts (light gray), including a surface profile (purple).

any existing patterned surface may be made resistant to shear-driven drainage: we predict that oil can be retained indefinitely if surface features are interrupted by periodic barriers with a period less than or equal to L_∞. For instance, if a grid of barriers with period L_∞ is overlaid on a random rough pattern, the surface will be expected to retain its lubricant up to the shear value used to determine L_∞. Such minimally structured geometries, designed according to the insights from this study, will allow for greater adoption of liquid-infused surfaces by enabling their use in applications where they would otherwise fail.

We thank C. Odier, R. Jeanneret, and D. Bartolo for helpful advice on implementing the microfluidic 'sticker' technique. In addition we thank Y. Fan and the staff of the Princeton Micro/Nano Fabrication Laboratory for assistance with microfabrication, and C. Arnold and J. Spechler for use of their confocal profilometer. This work was supported under ONR MURI Grants N00014-12-1-0875 and N00014-12-1- 0962 (Program Manager Dr. Ki-Han Kim). We thank all team members of our MURI program for their valuable feedback.

* hastone@princeton.edu

[1] T.-S. Wong, S. H. Kang, S. K. Y. Tang, E. J. Smythe, B. D. Hatton, A. Grinthal, and J. Aizenberg, Nature **477**, 443 (2011).
[2] A. Lafuma and D. Quéré, Europhysics Letters **96**, 56001 (2011).
[3] J. D. Smith, R. Dhiman, S. Anand, E. Reza-Garduno, R. Cohen, G. H. McKinley, and K. K. Varanasi, Soft Matter **9**, 1772 (2013).
[4] A. K. Epstein, T.-S. Wong, R. A. Belisle, E. M. Boggs, and J. Aizenberg, PNAS **109**, 13182 (2012).
[5] S. Anand, A. T. Paxson, R. Dhiman, J. D. Smith, and K. K. Varanasi, ACS Nano **6**, 10122 (2012).
[6] R. Xiao, N. Miljkovic, R. Enright, and E. N. Wang, Scientific Reports **3**, 1988 (2013).
[7] A. Busse, N. D. Sandham, G. McHale, and M. I. Newton, Journal of Fluid Mechanics **727**, 488 (2013).
[8] C. Schönecker, T. Baier, and S. Hardt, Journal of Fluid Mechanics **740**, 168 (2014).
[9] B. Solomon, K. Khalil, and K. Varanasi, Langmuir **30**, 10970 (2014).
[10] A. Lafuma and D. Quéré, Nature Materials **2**, 457 (2003).
[11] D. Bartolo, F. Bouamrirene, E. Verneuil, A. Buguin, P. Silberzan, and S. Moulinet, Europhysics Letters **74**, 299 (2006).
[12] D. Quéré, Annual Review of Materials Research **38**, 71 (2008).
[13] R. Poetes, K. Holtzmann, K. Franze, and U. Steiner, Physical Review Letters **105**, 166104 (2010).
[14] H.-M. Kwon, A. T. Paxson, K. K. Varanasi, and N. A. Patankar, Physical Review Letters **106**, 036102 (2011).
[15] P. Papadopoulos, L. Mammen, X. Deng, D. Vollmer, and H.-J. Butt, PNAS **110**, 3254 (2013).
[16] P. Lv, Y. Xue, Y. Shi, H. Lin, and H. Duan, Physical Review Letters **112**, 196101 (2014).
[17] B. J. Carroll, Colloids and Surfaces A **74**, 131 (1993).
[18] R. Salathiel, Journal of Petroleum Technology **25**, 1216 (1973).
[19] D. Khrustalev and A. Faghri, Journal of Heat Transfer **121**, 729 (1999).
[20] J. Suh, R. Greif, and C. Grigoropoulos, International Journal of Heat and Mass Transfer **44**, 3103 (2001).
[21] D. G. Sperry and R. J. Wassersug, The Anatomical Record **185**, 253 (1976).
[22] A. Allen and N. J. H. Carroll, Digestive Diseases and Sciences **30**, 55S (1985).
[23] J. Bico, C. Tordeux, and D. Quéré, Europhysics Letters **55**, 214 (2001).
[24] L. Courbin, E. Denieul, E. Dressaire, M. Roper, A. Ajdari, and H. A. Stone, Nature Materials **6**, 661 (2007).
[25] W. Liu, Y. Li, Y. Cai, and D. P. Sekulic, Langmuir **27**, 14260 (2011).
[26] M. M. Weislogel, Journal of Fluid Mechanics **709**, 622 (2012).
[27] E. Dressaire, L. Courbin, J. Crest, and H. A. Stone, Physical Review Letters **102**, 194503 (2009).
[28] J. Seiwert, M. Maleki, C. Clanet, and D. Quéré, Europhysics Letters **94**, 16002 (2011).
[29] R. Seemann, M. Brinkmann, E. J. Kramer, F. F. Lange, and R. Lipowsky, PNAS **102**, 1848 (2005).
[30] L. E. Stillwagon and R. G. Larson, Physics of Fluids A **2**, 1937 (1990).
[31] S. Kalliadasis, C. Bielarz, and G. M. Homsy, Physics of Fluids **12**, 1889 (2000).
[32] H. Luo and C. Pozrikidis, Journal of Fluid Mechanics **556**, 167 (2006).
[33] R. D. Lenz and S. Kumar, Physics of Fluids **19**, 102103 (2007).
[34] D. Bartolo, G. Degré, P. Nghe, and V. Studer, Lab on a Chip **8**, 274 (2008).
[35] See Supplemental Material [url], which includes Ref. [40].
[36] R. Lucas, Kolloid-Zeitschrift **23**, 15 (1918).
[37] E. W. Washburn, Physical Review **17**, 273 (1921).
[38] A. Carlson, P. Kim, G. Amberg, and H. A. Stone, Europhysics Letters **104**, 34008 (2013).
[39] S. Anand, K. Rykaczewski, S. B. Subramanyam, D. Beysens, and K. K. Varanasi, Soft Matter **11**, 69 (2014).
[40] R. K. Shah and A. L. London, *Laminar Flow Forced Convection in Ducts* (Academic Press, New York, NY, 1978).